



## Magnetic properties of novel dendrimeric spin crossover iron(III) complex



Natalia Domracheva<sup>a,\*</sup>, Valerya Vorobeva<sup>a</sup>, Andrew Pyataev<sup>b</sup>, Rui Tamura<sup>c</sup>, Katsuaki Suzuki<sup>c</sup>, Matvey Gruzdev<sup>d</sup>, Ulyana Chervonova<sup>d</sup>, Arkadij Kolker<sup>d</sup>

<sup>a</sup>Zavoisky Kazan Physical-Technical Institute, Russian Academy of Science, Sibirsky Tract 10/7, 420029 Kazan, Russia

<sup>b</sup>Kazan Federal University, Kremlyovskaya St. 18, 420008 Kazan, Russia

<sup>c</sup>Graduate School of Human and Environmental Studies, Kyoto University, Kyoto 606-8501, Japan

<sup>d</sup>G.A. Krestov Institute of Solution Chemistry, Russian Academy of Science, Akademicheskaya St. 1, 153045 Ivanovo, Russia

### ARTICLE INFO

#### Article history:

Received 22 June 2015

Received in revised form 16 October 2015

Accepted 16 October 2015

Available online 2 November 2015

Dedicated to the memory of Dr. R.A. Manapov.

#### Keywords:

Iron(III) complex

EPR spectroscopy

Mössbauer spectroscopy

Spin-crossover

Magnetic susceptibility

Dendrimers

### ABSTRACT

The synthesis and magnetic properties of novel dendrimeric spin crossover Fe(III) complex of formula  $[\text{Fe}(\text{L})_2]^+\text{PF}_6^-$ , where  $\text{L} = 3,5\text{-di}(3,4,5\text{-tris}(\text{tetradecyloxy})\text{benzoyloxy})\text{benzoyl-4-oxy-salicylidene-}N\text{-ethyl-}N\text{-ethylenediamine}$  have been studied for the first time by magnetic susceptibility, Electron Paramagnetic Resonance (EPR) and Mössbauer spectroscopy in the wide (2–300 K) temperature range. EPR showed that the compound is magnetically inhomogeneous, consists of two magnetic sub-lattices, displays a partial spin crossover ( $S = 5/2 \rightleftharpoons 1/2$ ) of ~25% of the Fe(III) molecules above 160 K and undergoes the antiferromagnetic (AF) ordering below 10 K. High-spin (HS,  $S = 5/2$ ) Fe(III) centers with weakly distorted octahedral environment most probably form chains in layers. The dimeric molecules, formed from low-spin (LS,  $S = 1/2$ ) centers and HS centers with strongly distorted octahedral environment are likely located between the layers and are involved in the spin crossover. EPR has shown the presence of AF dynamical spin clusters in the high temperature (70–300 K) range, which are visible in the short time scale ( $10^{-10}$  s) and could not be registered in the static magnetic measurements. Mössbauer spectra demonstrated in a paramagnetic state of the compound a quadrupole doublet with average isomer shift of 0.35 mm/s and splitting 0.72 mm/s corresponding to HS Fe(III) centers. Below 60 K, the spectra displayed the appearance of magnetic hyperfine structure, whose relaxation nature testifies the collective spin flips of small clusters in the material. Mössbauer spectroscopy confirmed the existence of AF ordering in the Fe(III) dendrimeric complex at 5 K.

© 2015 Elsevier B.V. All rights reserved.

### 1. Introduction

Designing magnetic materials with two or more potential functions arising from different physical properties has become a strong topic in chemical and materials science [1,2]. A wide choice of constituent molecules could allow the appearance in the same compound of unusual combination of physical properties. A suitable approach to obtain such a multifunctional material is the hybrid approach in which the material structure is constructed through self-assembly of two different molecular fragments having distinct properties. An interesting example is the multifunctional material that exhibits spin-crossover behavior with other physical properties [3–5]. Such synergic approach makes possible the production of systems in which one property may be controlled

by another. In this context, cationic spin-crossover (SCO) iron(III) complexes are suitable for this purpose. Iron(III) centers can adopt two different spin states, that is, low-spin (LS) and high-spin (HS) states that are interconvertible under an external stimulus such as temperature, pressure, light irradiation or solvents [6]. Considerable research efforts are focused to utilize the SCO phenomenon together with the non-linear optical properties [4], chirality [7], electrical conductivity [8] or long-range order [9].

The motivation for this work came from our desire to create a novel multifunctional material, in which spin-crossover phenomenon and magnetic ordering coexist. This strategy may open a way to design switching magnets in which the magnetic ordering of the system could be tuned, thus taking advantage of the possibility to induce the SCO phenomenon by applying the external stimuli such as light or pressure. However, this challenging goal requires first the preparation of such a material which is able to display the coexistence of spin crossover and magnetic ordering.

\* Corresponding author. Tel.: +7 (843) 2319065.

E-mail address: [ndomracheva@gmail.com](mailto:ndomracheva@gmail.com) (N. Domracheva).

Until now, work in this direction was carried out in the following way. The material structures have been constructed through the self-assembly of two different magnetic sub-lattices of transition metal ions having distinct properties. Namely, spin crossover (SCO) metal complexes have been integrated into 1D, 2D or 3D magnetically ordered sub-lattice of the other metal complexes. Examples of coexistence of the spin crossover behavior with magnetic ordering are very few today [10–12].

We suggest another way to obtain such bi-functional system: embedded SCO iron(III) complex into the focal point (core) of dendrimer molecule. This bi-functional system will be prepared by only one type of metal complexes. It is known that dendritic molecules can self-assemble into ordered supramolecular structures [13]. So, it can be expected that the self-organization of dendrons will generate a magnetic ordering in a system as it has been in the case of dendrimer-functionalized gold nanoparticles (NPs) showing ferromagnetism at room temperature [14].

In the present paper, we report about the unusual magnetic properties of spin-crossover dendrimeric iron(III) complex by EPR, Mössbauer spectroscopy and magnetic susceptibility, which demonstrate the coexistence of a partial spin crossover, magnetic ordering and AF dynamical spin clusters in the system.

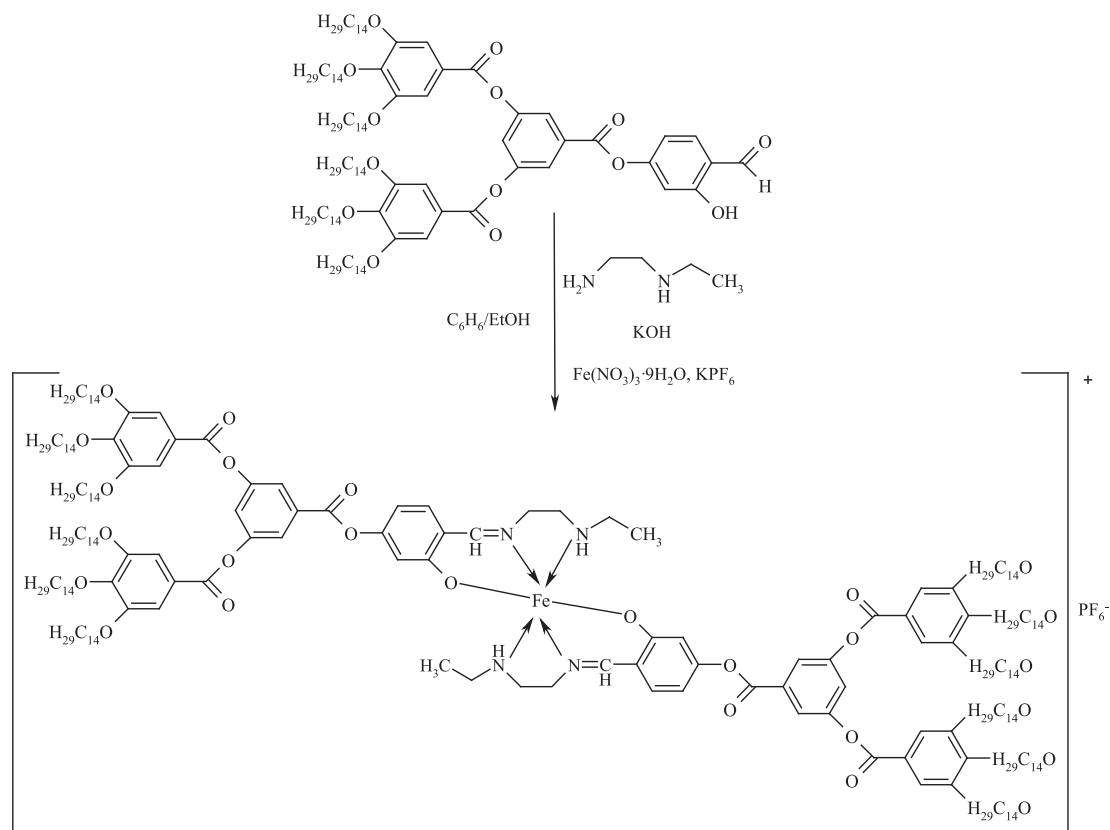
## 2. Results and discussion

### 2.1. Synthesis and Characterization of the dendritic iron(III) complex

The synthesis of iron(III) bis[3,5-di(3,4,5-tris(tetradecyloxy)benzyloxy)benzoyl-4-oxy-salicylidene-*N'*-ethyl-*N*-ethylenediamine] hexafluorophosphate complex was performed in accordance with Scheme 1; the details of synthesis are given in the Experimental Section. The synthesized compound was characterized by gel

permeation chromatography, elemental analysis, FT-IR, NMR spectroscopy and MALDI-ToF-MS method. The results of these methods permit us to construct the schematic model of the complex given in Scheme 1. Moreover, these data allowed one to conclude that the compound is a monocationic bis(ligand) Fe(III) complex of formula  $[\text{Fe}(\text{L})_2]^+\text{PF}_6^-$ , where iron(III) ion has an octahedral geometry with  $\text{N}_4\text{O}_2$  donor atoms formed by three atoms (ONN) of tridentate ligand (L). X-ray diffraction data obtained for similar  $[\text{Fe}(\text{Saen})_2]^+\text{Cl}^-$  complex but without dendritic periphery [15] showed that bis-tridentate ligands are arranged in a meridional (*mer*) configuration. DFT calculations [16] carried out for the full complex with dendritic environment confirmed that *mer* configuration of ligands is energetically most preferable. The optimized structure is shown in Fig. 1a.

Such a model of coordination polyhedron allows the formation of dimeric molecules, where iron ions are coupled by weak intermolecular interactions (H-bonds between the NRH fragments of the neighboring complexes and the anions) [15]. The possibility of the formation of such kind of dimeric molecules is also confirmed by quantum chemical calculations (Fig. 1b). Furthermore, X-ray diffraction data showed that  $[\text{Fe}^{\text{III}}(\text{Saen})_2]^+$  cations are packed in a chain forming layered structures [17] for  $[\text{Fe}^{\text{III}}(\text{Saen})_2]^+\text{ClO}_4^- \cdot 0.5\text{H}_2\text{O}$  compound and linked into a dimer [15,17] for complex  $[\text{Fe}^{\text{III}}(\text{Saen})_2]^+\text{ClO}_4^-$ , wherein anions are located between the cationic  $[\text{Fe}(\text{L})_2]^+$  fragments. It is not possible to grow a crystal and to get accurate crystallographic data for such a highly branched dendrimeric iron complex. Therefore, the X-ray powder diffractogram was measured on a sample at 300 K, which is shown in Fig. 2. The diffractogram demonstrates one intense low-angle peak and two broad halos in the region of the high angles. According to the results of studies of a similar iron mesogenic complex, this single low-angle peak probably indicates a layered structure [18].



**Scheme 1.** Schematic representation of the synthetic procedure and the model of Fe(III) complex with PF<sub>6</sub><sup>-</sup> counter ion.

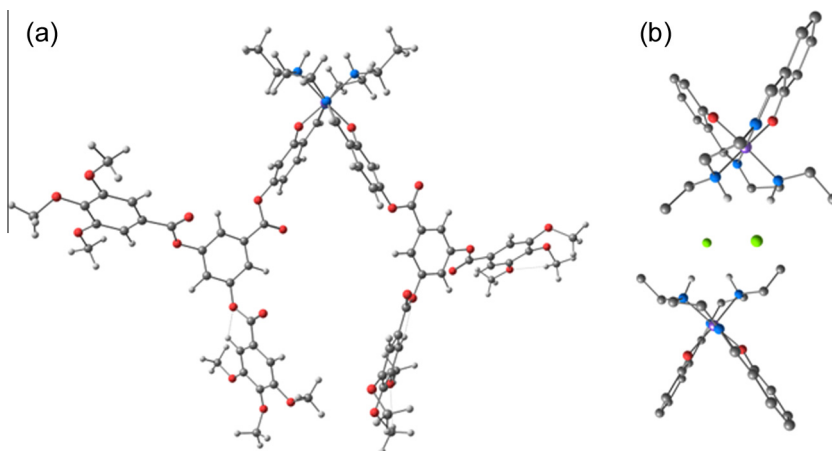


Fig. 1. The optimized structures of (a) Fe(III) complex and (b) dimeric molecule formed by two Fe(III) complexes and two chloride anions.

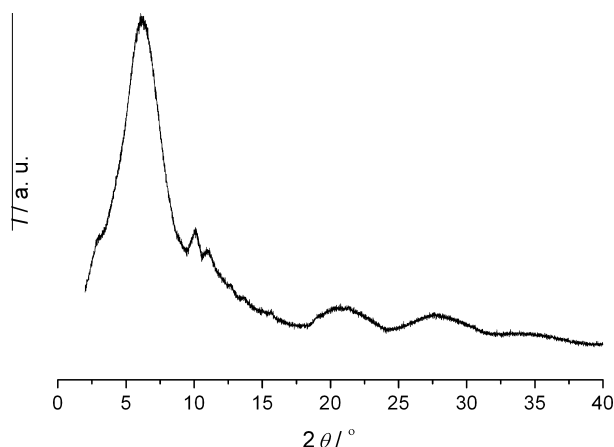


Fig. 2. X-ray diffractogram for the powder sample at room temperature.

The liquid crystalline properties of the compound were studied by differential scanning calorimetry and optical polarizing microscopy. It has been shown that above 317.3 K the complex exhibits mesomorphic properties and turns into isotropic liquid at 414.9 K.

## 2.2. Electron paramagnetic resonance

The temperature profile of the X-band EPR spectra ( $h\nu = 0.3 \text{ cm}^{-1}$ ) for the iron(III) dendrimeric complex measured in the region of 4.2–300 K are illustrated in Fig. 3. Three signals are observed in EPR spectra, one low-field signal with  $g_{\text{eff}} = 4.2$  and two high-field signals: the broad line with  $g_{\text{eff}} = 2$  and the axial signal with  $g_{\perp} = 2.208$ ,  $g_{\parallel} = 1.933$ .

The effective  $g$  values for high-spin (HS,  $S = 5/2$ ) Fe(III) centers are determined by zero-field splitting (ZFS) of the  ${}^6A$  electronic state. Wickman [19] and Aasa [20] have used the Hamiltonian (1)

$$\hat{H} = D \left( \hat{S}_z^2 - \frac{1}{3} S(S+1) \right) + E (\hat{S}_x^2 - \hat{S}_y^2) + g\beta\hat{H}\hat{S}, \quad (1)$$

to describe the combined effects of axial ZFS ( $D$ ), rhombic ZFS ( $E$ ) and the Zeeman interaction on the  ${}^6A$  electronic term. The positions of the fine structure lines in the spectrum depend on the value of the ratio between the microwave quantum  $h\nu$  and ZFS-parameters, which are induced by distortions of the crystal field in the compound. The  $g_{\text{eff}} = 4.2$  signal belongs to HS iron ions with strong ( $D \gg h\nu = 0.3 \text{ cm}^{-1}$ ) low-symmetry ( $E/D \sim 1/3$ ) crystal field (I-type of HS centers), whereas the broad  $g_{\text{eff}} = 2$  signal corresponds to HS

Fe(III) ions in an octahedral environment with weak ( $D \ll 0.3 \text{ cm}^{-1}$ ,  $E = 0$ ) distorted crystal field (II-type of HS centers). The axial resonance with  $g_{\perp} = 2.208$ ,  $g_{\parallel} = 1.933$  belongs to low-spin (LS,  $S = 1/2$ ) Fe(III) centers that have the  ${}^2T_{2g}$  ground state. It is important to note that the observation of distinct HS and LS EPR signals implies that the spin-state interconversion rates in the region of 4.2–300 K are slower relative to the X-band EPR time scale (ca.  $10^{-10} \text{ s}$ ).

The temperature dependence of the EPR lines integrated intensity ( $I$ ) is one of the sources of information about the spin transition process. The magnetic behavior of the compound reflected by the temperature dependencies of  $I$  and  $I \times T$  product of the whole EPR spectrum is shown in Fig. 4. One can see that the temperature dependence of  $I$  has complicated, two-step behavior: reaches the maximum at 10 K and then drops to the minimal value at about 70 K in the first temperature interval (4.2–70 K) and further begins to grow in the second temperature interval (70–300 K) (Fig. 4a). Variation of  $I \times T$  product from temperature (Fig. 4b) shows that the direct (4.2–300 K) and the inverse (300–4.2 K) thermal cycles practically coincide.

Let us try to understand the origin of the observed anomaly in our compound. For this purpose the temperature dependencies of the EPR lines integrated intensity were examined for each type of Fe(III) centers separately. The analysis of the EPR signals for each type of iron centers was based on the procedure of the model spectrum fitting to the observed experimental one. To fit the EPR spectra written in numerical format, we used the standard EasySpin-EPR spectrum simulation program. The parameters of the fit were the  $g$ - and  $D$ -tensor components, the line shape and the widths of the individual components  $\Delta H$ .

The first step is to turn our attention to the estimation of the fine structure parameter ( $D$ ) of the broad signal belonging to HS Fe(III) ions of the II-type (octahedral iron centers with weak axial distortion). A computer simulation of the broad signal indicates that the value of  $D$  should vary in the range  $0.02 \text{ cm}^{-1} < |D| < 0.03 \text{ cm}^{-1}$ . We used for the model spectrum fitting the absolute value of  $D = 0.025 \text{ cm}^{-1}$ , but a large number of different  $D$  values, belonging to the indicated range, can describe the broad signal (see Fig. 6b).

The simulated EPR spectra of the compound are depicted in Fig. 3 (see dashed lines) which have been calculated with the following magnetic parameters:  $g = 2.0$ ,  $D = 0.421 \text{ cm}^{-1}$ ,  $E = 0.109 \text{ cm}^{-1}$  for the I-type HS Fe(III) ions;  $g = 2.0$ ,  $D = 0.025 \text{ cm}^{-1}$  for the II-type of HS centers and  $g_{xy} = 2.208$ ,  $g_z = 1.933$  for the LS Fe(III) ions. The individual Lorentzian line shape was used for the simulation. As can be seen, a satisfactory

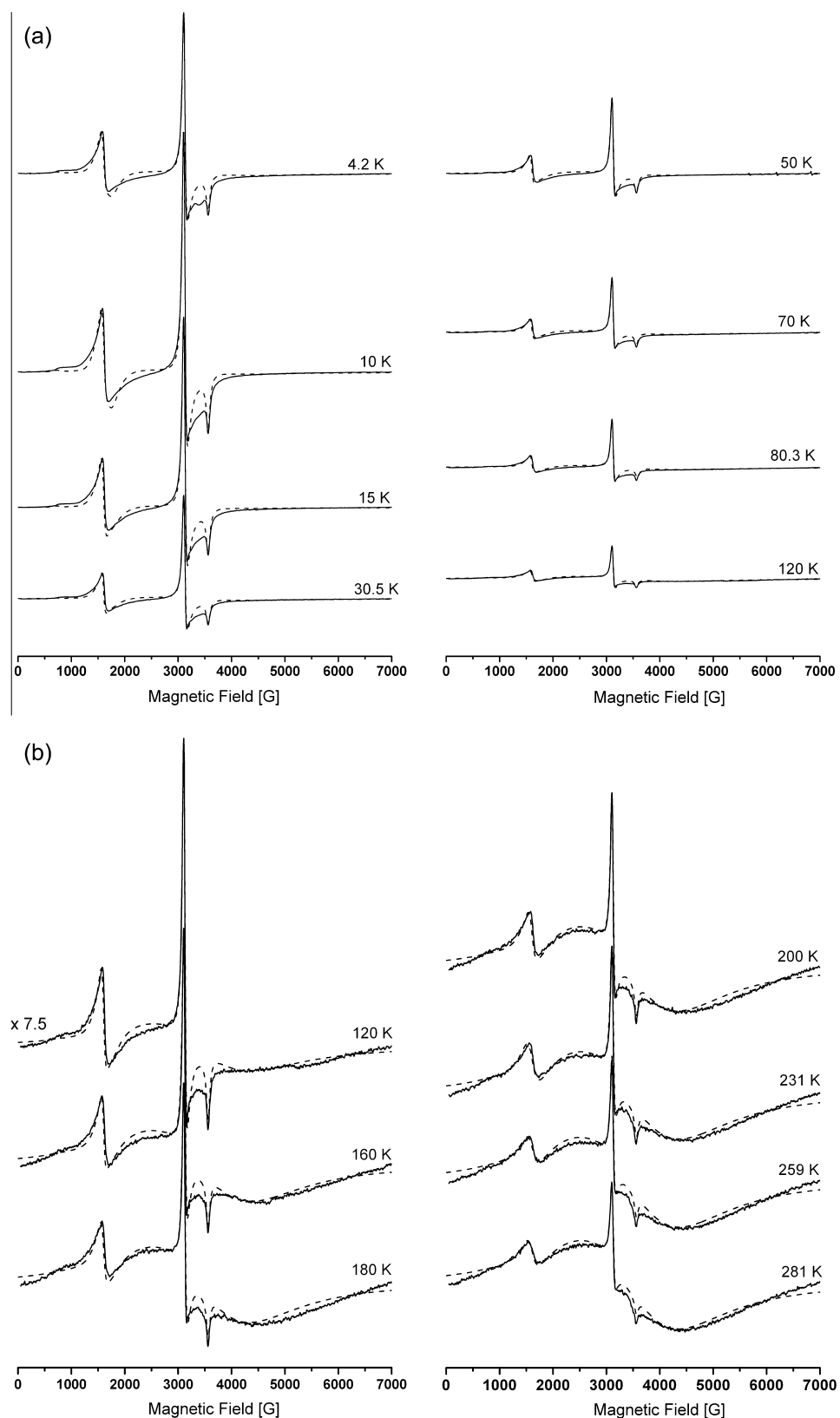


**Fig. 3.** The temperature dependence of the EPR spectra of the compound from (a) 4.2 to 120 K and (b) 120 to 281 K. Spectra in the temperature range (b) are recorded at higher amplification ( $\times 7.5$ ) in comparison with spectra in the range (a). The dashed lines show the theoretical EPR spectra.

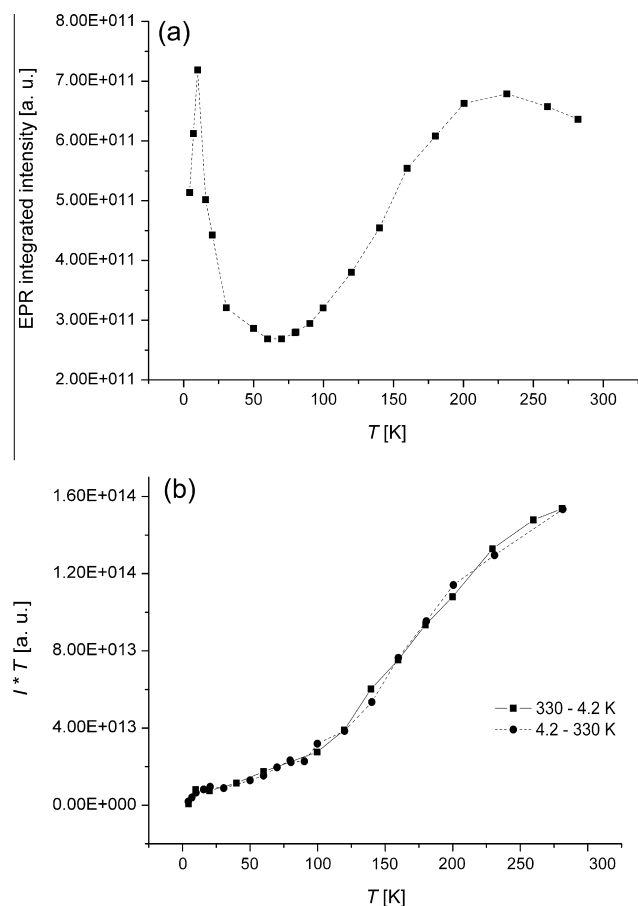


**Fig. 4.** (a) The temperature dependence of the EPR lines integrated intensity of the whole EPR spectrum. (b) The  $I \times T$  vs  $T$  plot.

agreement is obtained between the experimental and theoretical spectra.

Now let us analyze the EPR spectra of each type of iron(III) centers independently. Figs. 5–7 show the temperature variation of the EPR lines integrated intensities ( $I$ ),  $g$ ,  $\Delta H$  and ZFS-parameters values for the two types of HS and one LS centers, respectively. Note that the EPR lines integrated intensity ( $I$ ), which was obtained by numerical double integration of the first-derivative EPR spectrum, is proportional to the magnetic susceptibility. As can be seen, the temperature dependence of  $I$  for HS centers of the II-type ( $I_{HS,II}$ ) behaves in the opposite way compared with the EPR lines integrated intensities for the LS ( $I_{LS}$ ) and HS centers of the I-type ( $I_{HS,I}$ ).  $I_{HS,II}$  value grows with increasing temperature in the second (70–300 K) temperature interval and shows a broad maximum at about  $T_{max} \sim 259$  K, while the EPR lines integrated intensities of the other two iron(III) centers exhibit a sharp maximum at  $T_N = 10$  K and above  $T_N$ ,  $I_{LS}$  and  $I_{HS,I}$  follow the Curie–Weiss law up to 160 K. Such different behavior of iron centers indicates that there are two different magnetic sub-systems in the compound. According to the literature [21,22], a broad maximum in the magnetic susceptibility characterizes one-dimensional Heisenberg antiferromagnetic behavior, and it reflects the influence of the magnetic coupling along the chain of iron ions. It should be noted that the position of a broad maximum in the curve  $I$  vs.  $T$  essentially depends on the type of anion and the broad maximum shifts to lower temperatures  $T_{max} \sim 100$  K for Fe(III) complex with  $Cl^-$  counterion. Thus, we can assume that the broad resonance line at  $g \approx 2$  for the HS centers with weakly distorted coordination sphere arises from  $[Fe^{III}(L)_2]^+$  cations, packed in a chain forming a

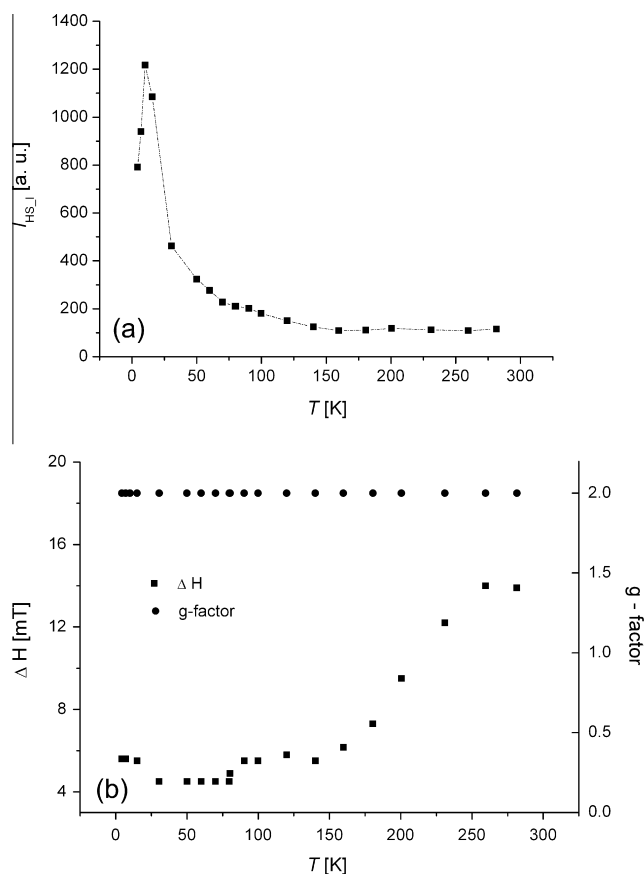


**Fig. 5.** (a) The temperature dependence of the EPR lines integrated intensity of the I-type HS iron(III) centers. (b) The temperature dependence of the  $g$ -factor and the width of the individual line of the I-type HS iron(III) centers.

layered structure. The number of these  $HS_{II}$  centers at room temperature is about 97%.

Let us analyze the results obtained for the other two iron centers. In accordance with the integrated intensity ratio, the number of LS to HS centers of the I-type is approximately 1:1 and is about 25% at  $T = 4.2$  K. The appearance of maximum on the curves  $I_{LS}$  and  $I_{HS,I}$  shows that LS–LS and  $HS_I$ – $HS_I$  iron centers are coupled by antiferromagnetic (AF) exchange interactions. The EPR magnetic data  $I_{LS}$  and  $I_{HS,I}$  vs.  $T$  between 4.2 and 90 K were analyzed with the spin–spin interaction model based on the exchange Hamiltonian  $H = -J S_A \cdot S_B$ . In the framework of a dimer model, the exchange constants  $J_{LS}$  and  $J_{HS,I}$  between LS–LS and  $HS_I$ – $HS_I$  centers were estimated with the help of Bleaney–Bowers equation [23] and Eq. (1) in [24], respectively. The best fit to the experimental data is displayed in Fig. 8a and b, that was obtained with  $J_{LS} = -13.1$  K and  $J_{HS,I} = -10.2$  K, respectively. Negative coupling constant  $J$  confirms the presence of the antiferromagnetic interactions between iron centers.

If we normalize the integrated intensity of each molecule fraction and superimpose these curves, the identical magnetic behavior for the LS and HS centers of the I-type is observed up to 160 K (see Fig. 8c), which follows the Curie–Weiss law above  $T_N$ . Above 160 K, the temperature dependencies of  $I_{LS}$  and  $I_{HS,I}$  deviate from the Curie–Weiss law: the number of HS centers of the I-type increases, while the number of LS centers decreases relative to the Curie–Weiss law. This fact means that a partial spin transition occurs in the compound between 160 and 300 K, where in a spin crossover ( $HS \rightleftharpoons LS$ ) takes part of  $\sim 25\%$  of the Fe(III) molecules. Since the behavior of LS and HS centers of the I-type

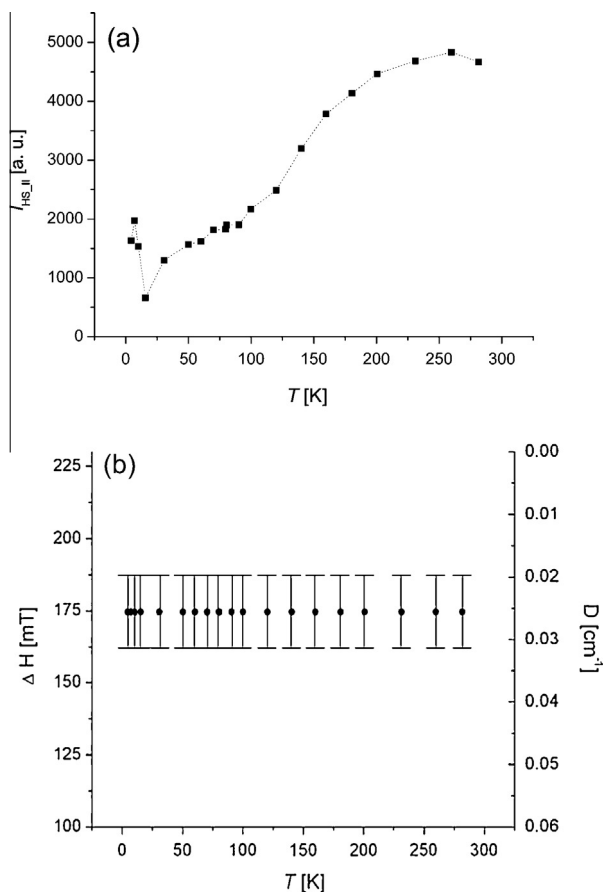


**Fig. 6.** (a) The temperature dependence of the EPR lines integrated intensity of the II-type HS iron(III) centers. (b) The range of  $D$ -values variation and the width of the individual line for the II-type HS iron(III) centers.

differs cardinally from the behavior of HS centers of the II-type, we can conclude that these centers are likely located between the layers.

Thus, the EPR results show that the studied magnetic  $[\text{Fe}(\text{L})_2]^+\text{PF}_6^-$  system is inhomogeneous and consists of two magnetic sub-lattices. The HS Fe(III) centers with weakly distorted octahedral environment most probably form chains in layers. LS–LS and HS–HS centers with strongly distorted octahedral environment form dimers, that are likely arranged between the layers and these centers are involved in a spin crossover. Example of such inhomogeneous magnetic system based on Fe(III) mesogen is known in the literature [25].

### 2.3. Magnetic susceptibility

The static magnetic susceptibility  $\chi$  for the powder sample was measured in a magnetic field of 5000 Oe as a function of temperature in the range 2–300 K. The measured data were corrected for the diamagnetic susceptibility ( $-0.000199$  emu) and for the sample holder contribution. Fig. 9a shows the temperature dependencies of the magnetic susceptibility and the effective magnetic moment ( $\mu_{\text{eff}}$ ), which demonstrates a decrease of the value from  $5.8 \mu_B$  at 300 K to  $2.4 \mu_B$  at 2.4 K.  $\mu_{\text{eff}}$  value at room temperature corresponds to the high-spin (HS) value of the Fe(III) ion ( $S = 5/2$ ,  $\mu_{\text{eff}} = 5.9 \mu_B$ ). The behavior of the inverse magnetic susceptibility versus  $T$  is presented in Fig. 9b. As can be seen, the Curie–Weiss law prevails above 10 K with constant  $\theta = -9.9$  K. The negative sign of  $\theta$  clearly indicates that antiferromagnetic interactions operate between Fe(III) ions.

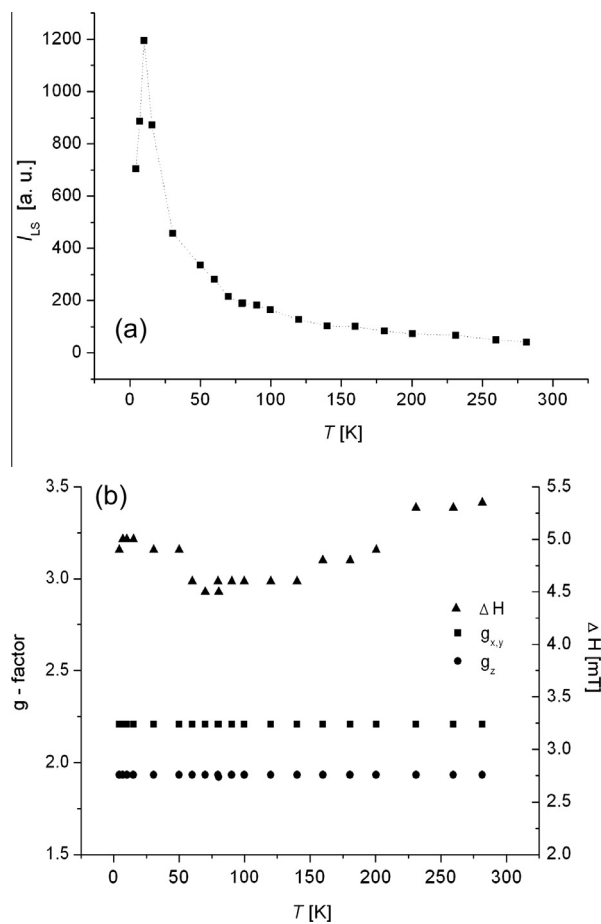


**Fig. 7.** (a) The temperature dependence of the EPR lines integrated intensity of the LS iron(III) centers. (b) The temperature dependence of the  $g$ -factor and the width of the individual line of the LS iron(III) centers.

A comparison of the temperature dependence of the static magnetic susceptibility (Fig. 9a) and the EPR integrated intensity (Fig. 4a) shows a large difference, especially in the high temperature range (70–300 K). These differences can be explained by regarding that  $I_{\text{HS,II}}$ , in contrast to the static magnetic susceptibility, reveals dynamic spin clusters at the EPR spectrometer frequency ( $\sim 9.4$  GHz). These antiferromagnetic (AF) spin clusters of short-range ordered spins are observed only on a short time scale ( $\tau = 1/\nu \sim 10^{-10}$  s) and could not be detected by method of static magnetic measurements. We suppose that the dynamic spin clusters represent nano-regions with antiferromagnetically correlated spins. Such nano-regions exist in the paramagnetic phase and behave themselves like superparamagnetic particles in the magnetic resonance spectrum. More clearly their behavior is observed in the iron(III) dendrimeric complex with chlorine counterion and this problem will be considered in our next publication. Application of the theory Raikher–Stepanov developed to superparamagnetic particles allow us to estimate the size and value of the anisotropy field of such nano-regions with antiferromagnetically correlated spins.

Note that for the first time the concept of dynamic spin clusters was proposed for the polycrystalline sample of  $\text{Zn}_3\text{Fe}_4\text{V}_6\text{O}_{24}$ , where the temperature dependence of the EPR integrated intensity of the broad line at  $g \approx 2.0$  showed a marked anomaly at about 220 K in contrast to the static magnetic susceptibility, where no such irregularity has been observed [26]. The authors explained the difference in behavior of  $I(T)$  and  $\chi(T)$  in the high temperature range

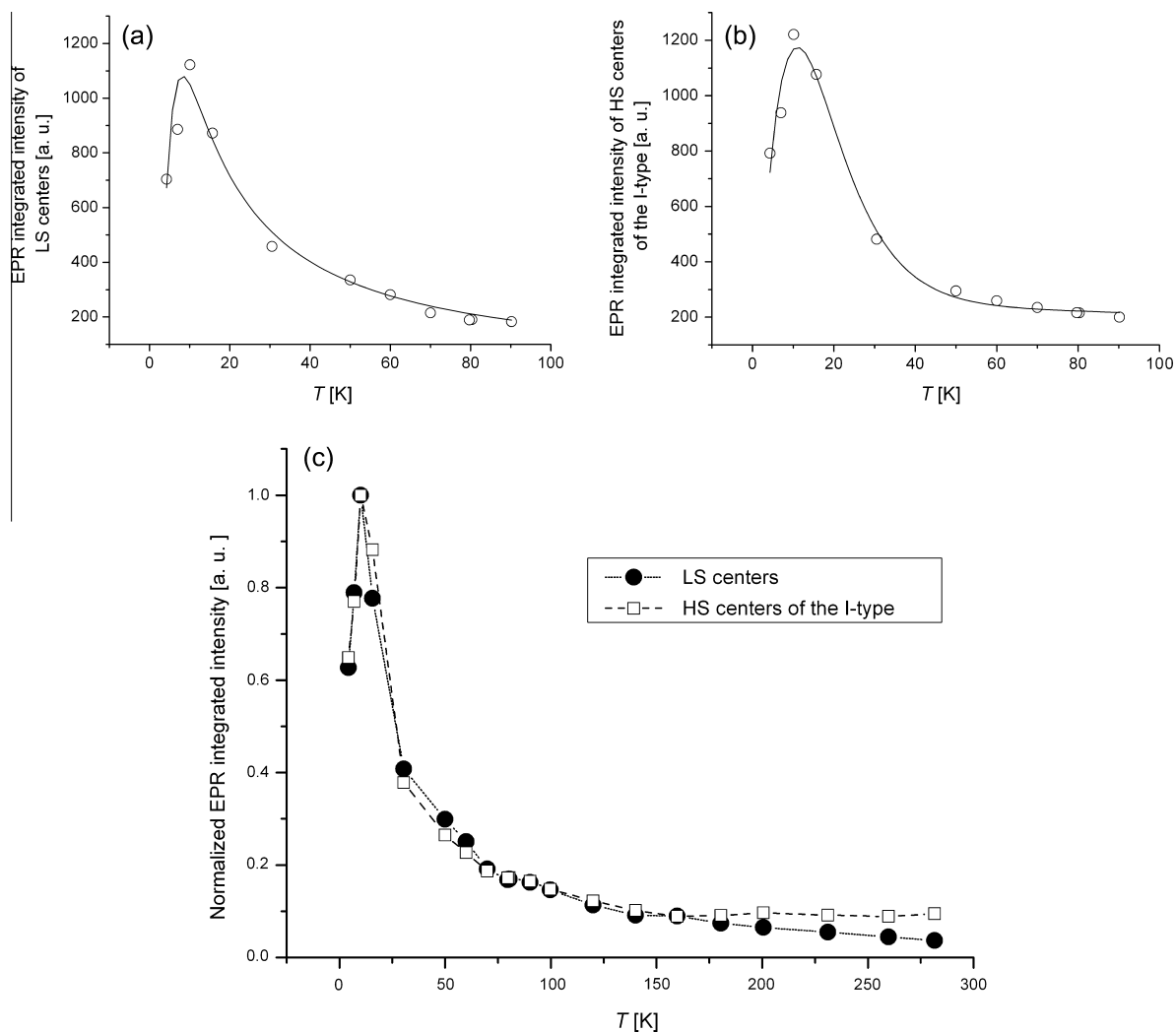


**Fig. 8.** The temperature dependence ( $4.2 \text{ K} \leq T \leq 90 \text{ K}$ ) of the EPR integrated intensity of the LS (a) and HS centers of the I-type (b). The solid lines represent the best fit to the experimental data with coupling constants mentioned in the text. (c) The temperature dependence of the EPR normalized integrated intensity of the LS and HS centers of the I-type at  $4.2 \text{ K} \leq T \leq 300 \text{ K}$ .

by means of AF dynamic spin clusters of short-range ordered spins existing only in the time scale of the EPR method of observation.

To confirm the concept of dynamic spin clusters which are present in our material, the Mössbauer spectroscopy studies were carried out, where the time scale of this method is  $\sim 10^{-7}$  s.

#### 2.4. Mössbauer spectroscopy study

Mössbauer spectra were measured in the temperature range 5–310 K. Spectrum recorded at 310 K (Fig. 10) consists of one broad doublet with parameters determined by the center of gravity method: isomer shift  $\delta_{\text{Fe}} = 0.35 \text{ mm/s}$  with respect to  $\alpha\text{-Fe}$  and quadrupole splitting  $Q_S = 0.72 \text{ mm/s}$ , which correspond to the high-spin (HS) state of the Fe(III) ion in an octahedral environment. It is known that the magnitude of the quadrupole splitting depends on the value of electric field gradient (EFG) on the  $^{57}\text{Fe}$  nucleus. EFG is formed by two contributions, the first one arises from the asymmetry of the electrons on the d-shell of Fe(III) ion. The second contribution comes from the atoms forming the coordination sphere of the iron ion. Fe(III) in HS state ( $S = 5/2$ ) has a symmetric, half-filled electron d-shell. Therefore,  $Q_S = 0.72 \text{ mm/s}$  value for our complex is mainly caused by distortions of the coordination polyhedron of

iron(III) centers. A good agreement between the experimental results and computer simulations can only be obtained by taking into account the distribution of the isomer shifts and quadrupole splittings. The distribution of the latter is the result of different distortions of Fe(III) coordination polyhedrons due to flexibility of dendrimeric ligands or due to anion site disorder between the neighboring iron centers.

One could expect to find a superposition of the quadrupole doublets of two spin states (HS and LS) at lower temperatures, as observed in the structurally similar complexes in [16]. However, only one quadrupole doublet with a broad line width is observed in the whole temperature range. This phenomenon indicates that the electronic relaxation time between the HS and LS state is faster than the lifetime of the nuclear excited states of iron-57 ( $0.98 \times 10^{-7}$  s) and the iron nucleus “sees” an average of the properties of both states, and that the values of the Mössbauer parameters are averaged and depend on the population of each form. The examples of such fast spin interconversion have been observed for many spin-crossover iron(III) complexes [27,28].

At the temperature below 60 K, a magnetic hyperfine structure ( $H_{\text{obs}} = 454.5 \text{ kG}$  at 5 K) appears in the spectrum and becomes more pronounced with further decrease of the temperature (Fig. 10).

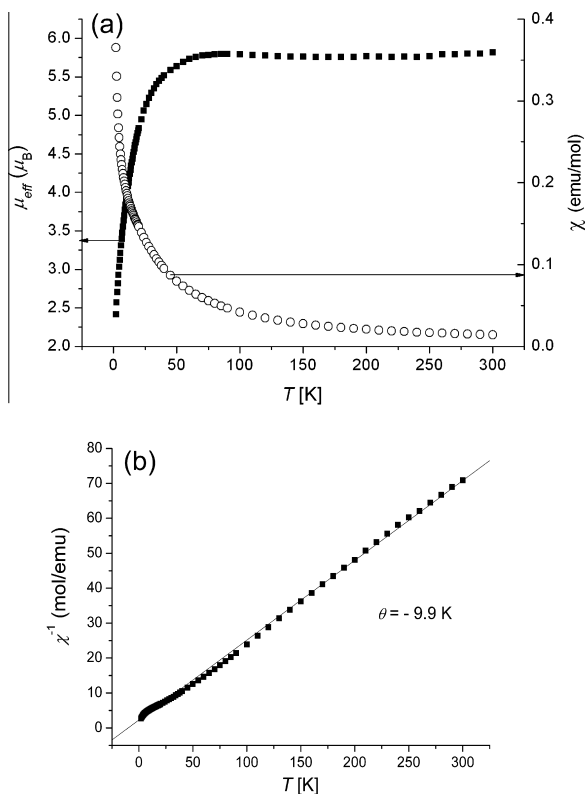


**Fig. 9.** (a) Temperature dependence of magnetic susceptibility  $\chi$  and effective magnetic moment for the studied compound. (b) Plot of the inverse magnetic susceptibility vs. temperature for the iron(III) complex. The solid line corresponds to the Curie–Weiss fit with  $\theta = -9.9$  K.

This indicates a process of magnetic spin correlations with frequency  $\nu < 10^7$  Hz of the spin fluctuations. At the same time, a small part of the quadrupole doublet remains in the spectra at 5 K. In the temperature range between 60 and 10 K, the hyperfine structure of spectra has a superparamagnetic-type of behavior [29]. The relaxation character of the hyperfine components is the result of collective spin flips of small clusters of the material [30]. So, below 60 K spectra demonstrate a magnetic phase transition from the paramagnetic state to antiferromagnetic (AF) type of ordering with a wide temperature range of superparamagnetism existence.

### 3. Conclusions

EPR, DC magnetic susceptibility and Mössbauer spectroscopy have been used to study the magnetism of spin-crossover dendrimeric iron(III) complex, which exhibits mesogenic properties. The system contains three types of magnetically active iron centers: one  $S = 1/2$  low-spin (LS) and two  $S = 5/2$  high-spin (HS) centers with strong ( $D = 0.421 \text{ cm}^{-1}$ ,  $E = 0.109 \text{ cm}^{-1}$ ) low-symmetry and weak ( $0.02 \text{ cm}^{-1} < |D| < 0.03 \text{ cm}^{-1}$ ) distorted octahedral environments. EPR has shown that the compound is magnetically heterogeneous and consists of two magnetic sub-lattices. The HS Fe(III) centers with weakly distorted octahedral environment most probably form chains in layers. The dimeric molecules, formed from LS–LS centers and HS–HS centers with strongly distorted octahedral environment, are likely located between the layers and are involved in the spin crossover that occurs in the range 160–300 K. EPR revealed the presence of the dynamical spin clusters in the high temperature (70–300 K) range, which are not detected by the DC magnetic susceptibility. Mössbauer spectra showed that the sample

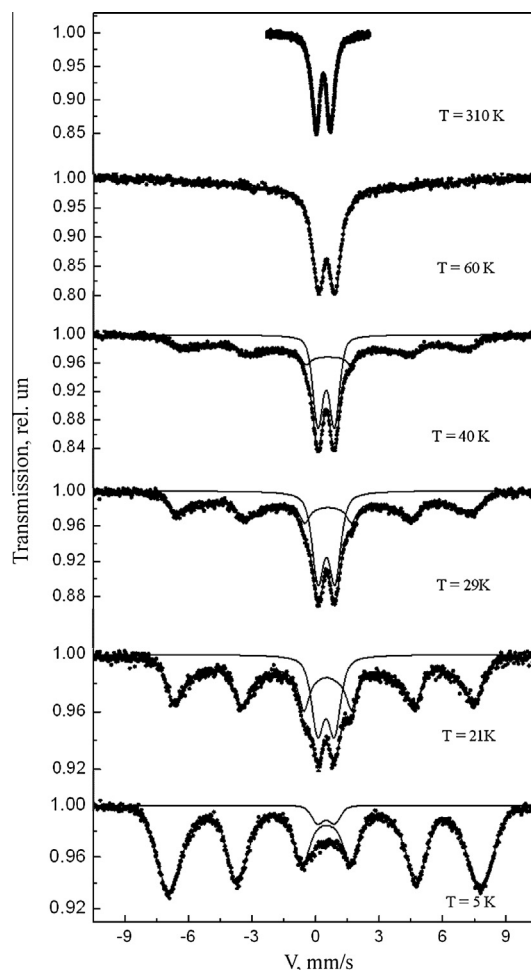


**Fig. 10.** Mössbauer transmission spectra of the compound at various temperatures.

in a paramagnetic phase consists of HS Fe(III) centers. Observation of distributions of the isomer shifts and quadruple splittings indicates the distortions of Fe (III) coordination polyhedrons. Below 60 K, the magnetic hyperfine structure appears in Mössbauer spectra and its relaxation nature testifies the collective spin flips of small clusters in the material. Antiferromagnetic ordering in the compound is observed at 5 K. The coexistence of magnetic ordering and a partial spin crossover has been detected for the first time in iron(III) dendrimeric complex.

### 4. Experimental

#### 4.1. Synthesis of dendrons derived from 3,4,5-tris(tetradecyloxy)benzoic acid

The ligand precursor 3,5-di[3,4,5-tris(tetradecyloxy)benzyloxy]-benzoyl-4-oxy-2-hydroxybenzaldehyde was prepared in accordance with reference [31,32] and Scheme A given in the Supporting Information. 3,4,5-Tris(tetradecyloxy)benzoic (**1**) acid was selected as the initial compound, and was synthesized in compliance with a standard method [33]. For the regular branching, the method of doubling the molecular size was employed, using the benzyl ester of 3,5-dihydroxybenzoic acid [34,35], which was synthesized by Chervonova et al. [34]. The esterification was carried out by interaction between the carboxyl and hydroxyl groups with the aid of dicyclohexylcarbodiimide in dichloromethane. The benzyl group was selectively removed by hydrogenolysis using 5% Pd/C as

catalyst in dry 1,4-dioxane [32,34,36]. The aldehyde was obtained by means of esterification of the corresponding acid and *para*-hydroxysalicylic aldehyde.

#### 4.2. Sample preparation and characterization

The synthesis of the complex was performed in accordance with Scheme 1. The reaction was carried out in binary solvent (benzene/ethanol). The formation of azomethine in solution and complexation by addition of iron(III) salt were confirmed by FT-IR spectroscopy and mass-spectrometry. Iron enriched to ~6% in  $^{57}\text{Fe}$  isotope was used to synthesize the complex. The substitution of the counter ion was carried out through the exchange reaction by adding a double excess of the potassium salt.

##### 4.2.1. Synthesis of iron(III) dendrimeric complex [31]

A portion of 3,5-di[3,4,5-tris(tetradecyloxy)benzoyloxy]benzoyl-4-oxy-2-hydroxy-benzaldehyde (0.5 g, 0.28 mmol) was dissolved in mixture of benzene and ethanol under constant stirring. *N*'-Ethyl-*N*-ethylenediamine (0.025 g, 0.28 mmol) and KOH (0.071 g, 1.28 mmol) dissolved in alcohol were added. Then the alcoholic solution of  $\text{Fe}(\text{NO}_3)_3 \cdot 9\text{H}_2\text{O}$  (0.057 g, 0.14 mmol) was added slowly drop by drop. After 15 min of stirring  $\text{KPF}_6$  (0.103 g, 0.56 mmol) dissolved in mixture of EtOH a few drops of water were slowly poured in it. The stirring was continued for 4 h. The precipitate was filtered off on a glass filter, washed by ethanol, and freeze-dried from benzene. The product is a finely dispersed brown powder. Yield is 0.46 g.

Found: C, 71.99; H, 10.13; N, 1.67. Calc. for  $\text{C}_{232}\text{H}_{390}\text{O}_{26}\text{N}_4$  Fe· $\text{PF}_6$ : C, 72.33; H, 10.20; N, 1.45.

FT-IR spectrum of complex,  $\nu_{\text{max}}/\text{cm}^{-1}$ : 3095w (Ph-H), 2921–2849s (Alk-H), 1729s (CO), 1591s (CN), 1002vs (NH), 857 w ( $\text{PF}_6^-$ ).

$^1\text{H}$  NMR spectrum of the complex registered in  $\text{CDCl}_3$  is paramagnetic which is registered as a few broad single peaks [37].

The complex was analyzed by gel permeation chromatography to establish of the chemical purity and homogeneity of the sample. Dry tetrahydrofuran was used as eluent. The chromatogram shows two peaks with different retention time ( $\tau_{\text{beg}1} = 8.27$  min,  $\tau_{\text{fin}1} = 8.72$  min;  $\tau_{\text{beg}2} = 8.73$  min,  $\tau_{\text{fin}2} = 9.27$  min) (see Fig. S1 in Supporting Information). The peak with  $\tau_1$  corresponds to supramolecular aggregates formed from the compound. Their formation can be explained by intermolecular interactions, where azomethine protons and  $\text{PF}_6^-$  counter ion are the bridging units. The second signal ( $\tau_2$ ) is identified as the peak of the individual target compound.

The presence of Schiff base and coordinated iron(III) ion in the structure of the complex was established by FT-IR spectroscopy. Two bands at ~5840 and ~5700  $\text{cm}^{-1}$  correspond to vibrations of tertiary and secondary amines [38] (see Fig. S2 in Supporting Information). A strong band at ~1585  $\text{cm}^{-1}$  is evidence of the  $-\text{CH}=\text{N}-$  bond occurrence which lies close to the absorption band of the carboxyl group  $\text{C}=\text{O}$  (1715–1730  $\text{cm}^{-1}$ ). Stretching vibrations of the Fe–O bond (422  $\text{cm}^{-1}$ ) and stretching vibrations of the Fe–N bond (584  $\text{cm}^{-1}$ ) are observed in the far range of infrared spectra [39–41].

A chelate compound with a high degree of branching does not give stable molecular ions, but it is fully fragmented within the range of  $m/z$  from 200 to 2000. The fragmentary ion with the value of  $m/z \sim 1861$   $[\text{L}+\text{K}]^+$  indicates Schiff base formation. Most intensity stable molecular ions are not observed even at change of matrix.

The liquid–crystalline properties of the compound were investigated by differential scanning calorimetry and optical polarizing microscopy. These data are available in the Supporting Information (see Fig. S3).

#### 4.3. Physical measurements

The EPR experiments were carried out on the powder sample. EPR studies were performed using X-band (9.41 GHz) CW-EPR EMXplus Bruker spectrometer that was provided with the helium ER 4112HV and the digital ER 4131VT temperature control systems. The accuracy of the reported magnetic parameters for LS iron complexes was  $\Delta g = \pm 0.005$  and  $\pm 0.005$  for the fine structure parameters. All Mössbauer spectra were obtained using a conventional constant-acceleration spectrometer where  $^{57}\text{Co}$  in Rh matrix was used as the source. The velocity calibration was obtained by using the  $\alpha$ -Fe spectrum. The isomer shift data were reported relative to the isomer shift of the  $\alpha$ -Fe spectrum. A liquid nitrogen continuous-flow cryostat was used for the temperature measurements in the range of 80–302 K. The lower temperature measurements were made using a helium cryostat. The Mössbauer absorber, which was prepared as a thin layer of powder between two aluminum foil discs, was mounted on the copper sample holder of the helium cryostat. The higher temperature measurements were made using a Mössbauer furnace. The temperature measurements and control were carried out by a type-T thermocouple and a heater above 50 K with the accuracy of 0.2 K. A carbon-resistance thermometer, calibrated at the liquid nitrogen and liquid helium temperatures, was used for the temperature measurements and control below 50 K with the accuracy of 0.5 K. Magnetic susceptibility measurements were carried out at heating rates of 2  $\text{K min}^{-1}$  in a 0.5 T magnetic field by means of a Quantum Design MPMS2 SQUID magnetometer. The experimental data were corrected for the diamagnetic contribution.

#### 4.4. DFT calculations

Geometry optimizations were performed within the PBE framework using the so-called 3z basis set of TZ2P quality (PRIRODA, version 5.0 package) [16].

#### Acknowledgments

We gratefully acknowledge the financial support for this work by RAS Presidium program No. 24, in part by the RFBR, project No 11-03-01028, grant of RFBR No. 14-03-31280-mol\_a and the grant of the President of the Russian Federation (No. MK-70.2014.3). We thank Prof. V.F. Tarasov and Dr. R.A. Manapov for fruitful discussions and remarks. EA, NMR, FT-IR spectroscopy and DSC analysis were carried out by the instrumentality of equipment of Interlaboratory scientific center “Verhnevolzhskij region center of physicochemical researching”.

#### Appendix A. Supplementary material

The results of synthesis of 3,5-di[3,4,5-tris(tetradecyloxy)benzoyloxy]benzoyl-4-oxy-2-hydroxybenzaldehyde, gel permeation chromatography, FT-IR spectroscopy, differential scanning calorimetry and optical polarizing microscopy are available. Supplementary data associated with this article can be found, in the online version, at <http://dx.doi.org/10.1016/j.ica.2015.10.024>.

#### References

- [1] E. Coronado, J.R. Galan-Mascaros, C.J. Gomez-Garcia, V. Laukhin, *Nature* 408 (2000) 447.
- [2] J.S. Miller, *Angew. Chem., Int. Ed.* 42 (2003) 27.
- [3] M.A. Halcrow, *Spin-crossover Materials: Properties and Applications*, Wiley, 2013.
- [4] A.B. Gaspar, V. Ksenofontov, M. Sereydyuk, P. Gutlich, *Coord. Chem. Rev.* 249 (2005) 2661.
- [5] M.C. Munoz, J.A. Real, *Coord. Chem. Rev.* 255 (2011) 2068.
- [6] M. Nihei, T. Shiga, Y. Maeda, H. Oshio, *Coord. Chem. Rev.* 251 (2007) 2606.

- [7] Y. Sunatsuki, Y. Ikuta, N. Matsumoto, H. Ohta, M. Kojima, S. Iijima, S. Hayami, Y. Maeda, S. Kaizaki, F. Dahan, J.P. Tuchagues, *Angew. Chem., Int. Ed.* **42** (2003) 1614.
- [8] K. Takahashi, H.B. Cui, Y. Okano, H. Kobayashi, H. Mori, H. Tajima, Y. Einaga, O. Sato, *J. Am. Chem. Soc.* **130** (2008) 6688.
- [9] M. Arai, W. Kosaka, T. Matsuda, S. Ohkoshi, *Angew. Chem., Int. Ed.* **47** (2008) 6885.
- [10] O. Roubeau, M. Evangelisti, E. Natividad, *Chem. Commun.* **48** (2012) 7604.
- [11] J.H. Yoon, D.W. Ryu, S.Y. Choi, H.C. Kim, E.K. Koh, J. Tao, C.S. Hong, *Chem. Commun.* **47** (2011) 10416.
- [12] M. Clemente-Leon, E. Coronado, M. Lopez-Jorda, G.M. Espallargas, A. Soriano-Portillo, J.C. Waerenborgh, *Chem. Eur. J.* **16** (2010) 2207.
- [13] J.I. Paez, M. Martinelli, V. Brunetti, M.C. Strumia, *Polymers* **4** (2012) 355.
- [14] B. Donnio, P. Garcia-Vazquez, J.L. Gallani, D. Guillon, E. Terazzi, *Adv. Mater.* **19** (2007) 3534.
- [15] A.P. Summerton, A.A. Diamantis, M.R. Snow, *Inorg. Chim. Acta* **27** (1978) 123.
- [16] N.E. Domracheva, A.V. Pyataev, V.E. Vorobeva, E.M. Zueva, *J. Phys. Chem. B* **117** (2013) 7833.
- [17] C.F. Sheu, S.M. Chen, G.H. Lee, Y.H. Liu, Y.S. Wen, J.J. Lee, Y.C. Chuang, Y. Wang, *Eur. J. Inorg. Chem.* **2013** (2013) 894.
- [18] M. Seredyuk, A.B. Gaspar, V. Ksenofontov, Y. Galyametdinov, J. Kusz, P. Gutlich, *Adv. Funct. Mater.* **18** (2008) 2089.
- [19] H.H. Wickman, M.P. Klein, *J. Chem. Phys.* **42** (1965) 2113.
- [20] R. Aasa, *J. Chem. Phys.* **52** (1970) 3919.
- [21] R.E. Caputo, R.D. Willett, *Phys. Rev. B* **13** (1976) 3956.
- [22] R. Dingle, M.E. Lines, *Phys. Rev. B* **187** (1969) 643.
- [23] R.L. Carlin, *Magnetochemistry*, Springer-Verlag, Berlin, 1985.
- [24] N. Guskos, G. Zolnierkiewicz, J. Typek, R. Szymczak, A. Blonska-Tabero, *Mater. Sci. Poland* **30** (2012) 1.
- [25] N.E. Domracheva, Yu.G. Galyametdinov, R.A. Manapov, A.V. Prosvirin, I.V. Ovchinnikov, *Phys. Solid State* **36** (1994) 1174.
- [26] J. Typek, G. Zolnierkiewicz, N. Guskos, R. Szymczak, A. Blonska-Tabero, *Rev. Adv. Mater. Sci.* **23** (2010) 207.
- [27] H. Ohshio, Y. Maeda, Y. Takashima, *Inorg. Chem.* **22** (1983) 2684.
- [28] Y. Maeda, N. Tsutsumi, Y. Takashima, *Inorg. Chem.* **23** (1984) 2440.
- [29] J.L. Dormann, D. Fiorani, E. Tronc, *Adv. Chem. Phys.* **98** (1997) 283.
- [30] L.M. Levinson, M. Luban, S. Shtrikman, *Phys. Rev.* **177** (1969) 864.
- [31] U.V. Chervonova (Ph.D. thesis), G.A. Krestov Institute of Solution Chemistry of RAS, Ivanovo, 2012.
- [32] U. Gruzdev, O. Chervonova, A. Akopova, Kolker, *J. Chem. Sci.* **127** (2015), <http://dx.doi.org/10.1007/s12039-015-0945-4> (in press).
- [33] A. Schaz, E. Valaityte, G. Lattermann, *Liq. Cryst.* **32** (2005) 513.
- [34] U.V. Chervonova, M.S. Gruzdev, A.M. Kolker, *Rus. J. Gen. Chem.* **81** (2011) 2288.
- [35] C. Saudan, V. Balzani, M. Gorka, S.-K. Lee, M. Maestri, V. Vicinelli, F. Vögtle, *J. Am. Chem. Soc.* **125** (2003) 4424.
- [36] H.N.S. Murthy, B.K. Sadashiva, *Liq. Cryst.* **31** (2004) 1347.
- [37] P. Gütllich, E. Bill, A.X. Trautwein, in: P. Gütllich, E. Bill, A.X. Trautwein (Eds.), *Mössbauer Spectroscopy and Transition Metal Chemistry*, Springer, Berlin, 2011, p. 568.
- [38] I.A. Vechkasov, N.A. Kruchinin, A.I. Polyakov, V.F. Rezinkin, in: L.N. Laricheva (Ed.), *Devices and Methods of Analysis in the Near IR Range*, Khimiya, Moscow, 1977, p. 280.
- [39] K. Nakamoto, in: K. Nakamoto (Ed.), *IR Spectra of Inorganic and Coordination Compounds*, Mir, Moscow, 1991, p. 536.
- [40] A. Finch, P. Geits, K. Redclif, F. Dickson, F. Bentley, in: F. Bentley (Ed.), *Chemical Application of Far Infrared Spectroscopy*, Academic Press, London, 1970, p. 277.
- [41] I.M. Cheremisina, *J. Struct. Chem.* **19** (1978) 336.